Channel Shaping Using Reconfigurable Intelligent Surfaces: From Diagonal to Beyond

Yang Zhao, *Member, IEEE,* Hongyu Li, *Graduate Student Member, IEEE,*
Massimo Franceschetti, *Fellow, IEEE,* and Bruno Clerckx, *Fellow, IEEE*

***Abstract*—This paper investigates how a passive Reconfigurable Intelligent Surface (RIS) can reshape the Multiple-Input Multiple-Output (MIMO) point-to-point channel in terms of singular values. We depart from the widely-adapted diagonal phase shift model to a general Beyond-Diagonal (BD) architecture, which provides superior shaping capability thanks to in-group connections between elements. An efficient Riemannian Conjugate Gradient (RCG) algorithm is tailored for smooth optimization problems of asymmetric BD-RIS with arbitrary group size, then invoked for the Pareto frontier of channel singular values. To understand the gain from off-diagonal entries, we also derive analytical singular value bounds in Line-of-Sight (LoS) and fully-connected scenarios. As a side product, we tackle MIMO rate maximization problem by alternating between active beamformer (eigenmode transmission) and passive beamformer (RCG algorithm) until convergence. A low-complexity suboptimal solution based on channel shaping is also proposed, where the decoupled problem is formulated as channel power maximization and solved in closed form iteratively. Theoretical analysis and numerical evaluation reveal that the shaping advantage of BD-RIS increases with group size and MIMO dimensions, stemming from stronger subchannel rearrangement and subspace alignment capabilities.**

***Index Terms*—Reconfigurable intelligent surface, multi-input multi-output, manifold optimization, singular value control, rate maximization.**

I. Introduction

Today we are witnessing a paradigm shift from connectivity to intelligence, where the wireless environment is no longer a chaotic medium but a conscious agent that serves on demand. This is empowered by the recent advances in Reconfigurable Intelligent Surface (RIS), a real-time programmable metasurface of numerous non-resonant sub-wavelength scattering elements. It can manipulate the amplitude, phase, frequency, and polarization of the scattered waves [1] with a higher energy efficiency, lower cost, lighter footprint, and greater scalability than relays. Using RIS for passive beamforming has attracted significant interest in wireless communication [2]–[5], backscatter [6], [7], sensing [8], [9], and power transfer literature [10]–[12], reporting a second-order array gain and fourth-order power scaling law (with proper waveform). On the other hand, RIS also enables backscatter modulation by dynamically switching between different patterns, as already investigated [13]–[15] and prototyped [16], [17]. Despite fruitful outcomes, one critical unanswered question is the channel shaping capability: *To what extent can a passive RIS reshape the wireless channel?*

The answer indeed depends on the hardware architecture and scattering model. In conventional (a.k.a. diagonal) RIS, each scattering element is tuned by a dedicated impedance and acts as an *individual* phase shifter [18]. The concept is generalized to Beyond-Diagonal (BD)-RIS [19], [20] which groups adjacent elements using passive components. This allows *cooperative* scattering — wave impinging on one element can propagate within the circuit and depart partially from any element in the same group. BD-RIS can thus control both amplitude and phase of the reflected wave, generalizing the scattering matrix from diagonal with unit-magnitude entries to block diagonal with unitary blocks. Its benefit has been recently shown in receive power maximization [21]–[24], transmit power minimization [25], and rate maximization [24]–[28]. Practical issues such as channel estimation [29] and mutual coupling [30] have also been investigated. Therefore, BD-RIS is envisioned as the next generation channel shaper with stronger signal processing flexibility [31].

Channel shaping is different from passive beamforming as it seeks to modify the inherent properties of the channel itself. This allows one to decouple the RIS-transceiver design and explore the fundamental limits of channel manipulation. For example, diagonal RIS has been proved useful for improving channel power [32], degree of freedom [33], [34], condition number [35], [36], and effective rank [37], [38] in Multiple-Input Multiple-Output (MIMO). In contrast, BD-RIS can provide a higher channel power but existing results are limited to Single-Input Single-Output (SISO)[1]. [21] and Multiple-Input Single-Output (MISO) [22]. While these studies offer promising glimpses into the channel shaping potential, a comprehensive understanding of the capabilities and limitations is desired, and a universal design framework is missing. This paper aims to answer the channel shaping question through theoretical analysis and numerical optimization. The contributions are summarized below.

First, we quantify the capability of a BD-RIS to reshape the MIMO point-to-point channel in terms of singular values. The *Pareto frontiers* are characterized by optimizing the weighted sum of singular values, where the weights can be positive, zero, or negative. The resulting region generalizes most relevant metrics and provides an intuitive channel shaping benchmark. We then discuss some analytical singular value bounds in Line-of-Sight (LoS) and fully-connected scenarios, which help to demystify the gain from off-diagonal entries. This is the first paper to answer the channel shaping question and highlight the BD-RIS gain from a Pareto perspective.

Second, we propose a Riemannian Conjugate Gradient (RCG) algorithm for smooth optimization problems of asymmetric BD-RIS with arbitrary group size. Specifically,

[1]In terms of channel shaping, single-stream MIMO with given precoder and combiner [21] is equivalent to SISO.

block-wise update is performed along the geodesics[2] and evaluated compactly by the exponential map. The proposed method features lower complexity and faster convergence than general manifold optimization [39], [40], and is used to solve the Pareto singular value problem. This is the first paper to tailor an efficient optimization framework that unleashes the design potential of asymmetric BD-RIS.

Third, we tackle BD-RIS MIMO rate maximization with two solutions: a local-optimal approach through Alternating Optimization (AO) and a low-complexity approach over channel shaping. The former updates active and passive beamformers by eigenmode transmission and RCG algorithm, respectively. The latter suboptimally decouples both blocks, recasts the shaping problem as channel power maximization, and solves it in closed form iteratively. Interestingly, the gap vanishes as BD-RIS evolves from diagonal (single-connected) to unitary (fully-connected). It suggests that channel shaping offers a crucial guideline for joint RIS-transceiver designs.

Fourth, extensive simulations reveal that the advantage of BD-RIS increases with group size and MIMO dimensions. In terms of channel power, fully-connected BD-RIS boosts up to 62%, 312%, 537% over single-connected in 1×1, 4×4, 16×16 configuration under Rayleigh fading. The superiority stems from stronger *subchannel rearrangement* and *subspace alignment* capabilities empowered by in-group cooperation. It emphasizes the importance of BD-RIS in large-scale MIMO systems.

Notation: Italic, bold lower-case, and bold upper-case letters indicate scalars, vectors and matrices, respectively. $\jmath$ denotes the imaginary unit. $\mathbb{C}$ represents the set of complex numbers. $\mathbb{U}^{n\times n}$ denotes the set of $n\times n$ unitary matrices. $\mathbf{0}$ and $\mathbf{I}$ are the all-zero and identity matrices with appropriate size, respectively. $\mathrm{tr}(\cdot)$ and $\det(\cdot)$ evaluates the trace and determinant of a square matrix, respectively. $\mathrm{diag}(\cdot)$ constructs a square matrix with arguments on the main diagonal and zeros elsewhere. $\mathrm{sv}(\cdot)$ returns the singular value vector. $\sigma_n(\cdot)$ and $\lambda_n(\cdot)$ is the n-th largest singular value and eigenvalue, respectively. $(\cdot)^*$, $(\cdot)^{\mathsf{T}}$, $(\cdot)^{\mathsf{H}}$, $(\cdot)^{(r)}$, $(\cdot)^\star$ denote the conjugate, transpose, conjugate transpose, r-th iterated, and final results, respectively. $|\cdot|$ denotes the absolute value. $\|\cdot\|_p$ means the p-norm and $\|\cdot\|$ suggests $p=2$. $\|\cdot\|_{\mathrm{F}}$ represents the Frobenius norm. $\sim$ means "distributed as". $\mathcal{CN}(\mathbf{0},\mathbf{\Sigma})$ is the multivariate Circularly Symmetric Complex Gaussian (CSCG) distribution with mean $\mathbf{0}$ and covariance $\mathbf{\Sigma}$.

II. BD-RIS Model

Consider a BD-RIS aided point-to-point MIMO system with N_{T}, N_{S}, N_{R} transmit, scatter, and receive antennas, respectively. This configuration is denoted as $N_{\mathrm{T}}\times N_{\mathrm{S}}\times N_{\mathrm{R}}$. The BD-RIS is modeled as an N_{S}-port network [41] that further divides into G independent groups. Each group contains $L\triangleq N_{\mathrm{S}}/G$ elements interconnected by real-time reconfigurable components [19]. To simplify the analysis, we assume the BD-RIS features lossless asymmetric[3] in-group connections without mutual coupling. The overall scattering matrix is thus block diagonal $\mathbf{\Theta}=\mathrm{diag}(\mathbf{\Theta}_1,\ldots,\mathbf{\Theta}_G)\in\mathbb{U}^{N_{\mathrm{S}}\times N_{\mathrm{S}}}$, where $\mathbf{\Theta}_g\in\mathbb{U}^{L\times L}$ is a unitary matrix corresponding to group $g\in\mathcal{G}\triangleq\{1,\ldots,G\}$. Consider a quasi-static block fading model where $\mathbf{H}_{\mathrm{D}}\in\mathbb{C}^{N_{\mathrm{R}}\times N_{\mathrm{T}}}$, $\mathbf{H}_{\mathrm{F}}\in\mathbb{C}^{N_{\mathrm{S}}\times N_{\mathrm{T}}}$, $\mathbf{H}_{\mathrm{B}}\in\mathbb{C}^{N_{\mathrm{R}}\times N_{\mathrm{S}}}$ denote the direct (transmitter-receiver), forward (transmitter-RIS), and backward (RIS-receiver) channels, respectively. The equivalent channel is

$$\mathbf{H}=\mathbf{H}_{\mathrm{D}}+\mathbf{H}_{\mathrm{B}}\mathbf{\Theta}\mathbf{H}_{\mathrm{F}}=\mathbf{H}_{\mathrm{D}}+\sum_g\mathbf{H}_{\mathrm{B},g}\mathbf{\Theta}_g\mathbf{H}_{\mathrm{F},g},\tag{1}$$

where $\mathbf{H}_{\mathrm{B},g}\in\mathbb{C}^{N_{\mathrm{R}}\times L}$ and $\mathbf{H}_{\mathrm{F},g}\in\mathbb{C}^{L\times N_{\mathrm{T}}}$ are the backward and forward channels of RIS group g, respectively.

Remark 1. *BD-RIS reduces to diagonal RIS and unitary RIS with group size 1 and N_{S}, respectively.*

Remark 2. *Individual forward and backward Channel State Information (CSI) are required for BD-RIS designs. This is different from diagonal RIS where estimating their product is usually sufficient. Later we will show the potential benefits from the CSI overhead.*

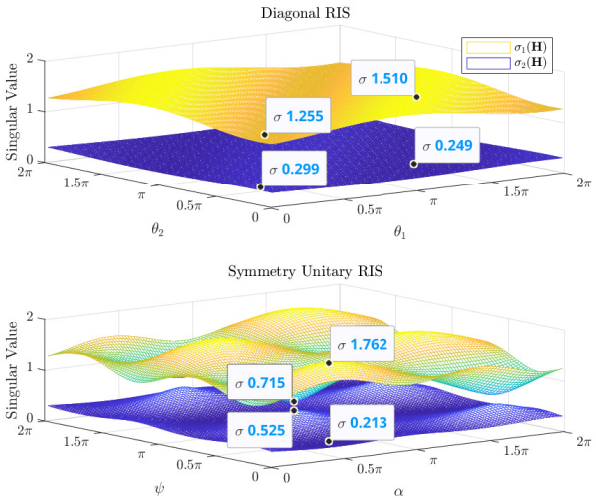

Fig. 1. Channel singular value shaping by diagonal and symmetry unitary RIS. $(N^{\mathrm{T}},N^{\mathrm{S}},N^{\mathrm{R}})=(2,2,2)$. Direct link is absent.

III. Channel Singular Value Redistribution

A. A Toy Example

We first illustrate the channel shaping capabilities of different RIS by a toy example. Consider a $2\times2\times2$ setup where the direct link is blocked. The diagonal RIS is modeled by $\mathbf{\Theta}_{\mathrm{D}}=\mathrm{diag}(e^{\jmath\theta_1},e^{\jmath\theta_2})$ while the unitary BD-RIS has 4 independent angular parameters

$$\mathbf{\Theta}_{\mathrm{U}}=e^{\jmath\phi}\begin{bmatrix}e^{\jmath\alpha}\cos\psi & e^{\jmath\beta}\sin\psi\\ -e^{-\jmath\beta}\sin\psi & e^{-\jmath\alpha}\cos\psi\end{bmatrix}.\tag{2}$$

In particular, ϕ has no impact on the singular value because $\mathrm{sv}(e^{\jmath\phi}\mathbf{A})=\mathrm{sv}(\mathbf{A})$. For a fair comparison, we also consider symmetric impedance network with $\beta=\pi/2$. Fig. 1 shows the channel singular values achieved by an exhaustive grid search over (θ_1,θ_2) for diagonal RIS and (α,ψ) for symmetric unitary

[2]A geodesic refers to the shortest path between two points in a Riemannian manifold.

[3]While symmetric impedance network is often considered in the literature [19], [21]–[27], asymmetric passive components (e.g., ring hybrids and branch-line hybrids) may also be reconfigured in real time [42]. Asymmetric BD-RIS has been discussed in [20], [27], [28].

Algorithm 1: Block-wise RCG update for asymmetric BD-RIS

Input: $f(\boldsymbol{\Theta})$, G
Output: $\boldsymbol{\Theta}^\star$
$r \leftarrow 0$, $\boldsymbol{\Theta}^{(0)}$
Repeat
  $r \leftarrow r+1$
  For $g \leftarrow 1$ to G
    $\nabla_{\mathrm{E},g}^{(r)} \leftarrow \partial f(\boldsymbol{\Theta}_g^{(r)})/\partial \boldsymbol{\Theta}_g^*$
    $\nabla_{\mathrm{R},g}^{(r)} \leftarrow \nabla_{\mathrm{E},g}^{(r)} \boldsymbol{\Theta}_g^{(r)\mathsf{H}} - \boldsymbol{\Theta}_g^{(r)} \nabla_{\mathrm{E},g}^{(r)\,\mathsf{H}}$
    $\gamma_g^{(r)} \leftarrow \mathrm{tr}\big((\nabla_{\mathrm{R},g}^{(r)} - \nabla_{\mathrm{R},g}^{(r-1)}) \nabla_{\mathrm{R},g}^{(r)\,\mathsf{H}}\big) / \mathrm{tr}\big(\nabla_{\mathrm{R},g}^{(r-1)} \nabla_{\mathrm{R},g}^{(r-1)\mathsf{H}}\big)$
    $\mathbf{D}_g^{(r)} \leftarrow \nabla_{\mathrm{R},g}^{(r)} + \gamma_g^{(r)} \mathbf{D}_g^{(r-1)}$
    $\mu_g^{(r)} \leftarrow \mathrm{argmax}_{\mu_g} f\big(\exp(\mu_g \mathbf{D}_g^{(r)}) \boldsymbol{\Theta}_g^{(r)}\big)$
    $\boldsymbol{\Theta}_g^{(r+1)} \leftarrow \exp\big(\mu_g^{(r)} \mathbf{D}_g^{(r)}\big) \boldsymbol{\Theta}_g^{(r)}$
  End For
Until $|R^{(r)} - R^{(r-1)}|/R^{(r-1)} \le \epsilon$

RIS. Interestingly, both singular values can be manipulated up to 9% using diagonal RIS and 42% using symmetric BD-RIS, despite both architectures have the same number of angular parameters and scattering elements. A larger performance gap is expected when asymmetric BD-RIS is available. This example shows BD-RIS can provide a wider dynamic range of channel singular values. It emphasizes the importance of cooperative scattering and motivates further studies on channel shaping.

B. Pareto Frontier Characterization

We then characterize the Pareto frontier of channel singular values by maximizing their weighted sum

$$\max_{\boldsymbol{\Theta}} \quad \sum_n \rho_n \sigma_n(\mathbf{H}) \tag{3a}$$

$$\text{s.t.} \quad \boldsymbol{\Theta}_g^{\mathsf{H}} \boldsymbol{\Theta}_g = \mathbf{I}, \quad \forall g, \tag{3b}$$

where $n \in \{1,\ldots,\min(N_{\mathrm{T}},N_{\mathrm{R}})\}$ and ρ_n is the weight of the n-th singular value that can be positive, zero, or negative. Varying $\{\rho_n\}$ allows us to explore the entire achievable singular value region. Problem (3) thus generalizes all relevant metrics and provides a powerful channel shaping framework. For group g, the objective is smooth in $\boldsymbol{\Theta}_g$ and the feasible domain corresponds to the Stiefel manifold. Those properties motivate us to zoom out to general smooth optimization problems of asymmetric BD-RIS with arbitrary group size.

Inspired by [43], [44], we propose a block-wise RCG update along the geodesics on the Lie group of unitary matrices $\mathbb{U}^{L\times L}$. The gradient

For general optimization problems with block unitary constraint, the adapted RCG method at iteration r for block g is summarized below, where $f\big(\boldsymbol{\Theta}_g^{(r)}\big)$ is the objective function also evaluated over $\big\{\{\boldsymbol{\Theta}_{g'}^{(r+1)}\}_{g'<g}, \{\boldsymbol{\Theta}_{g'}^{(r)}\}_{g'>g}\big\}$.

1) Compute the Euclidean gradient

$$\nabla_g^{\mathrm{E}(r)} = \frac{\partial f\big(\boldsymbol{\Theta}_g^{(r)}\big)}{\partial \boldsymbol{\Theta}_g^*}; \tag{4}$$

2) Translate to the Riemannian gradient

$$\nabla_g^{\mathrm{R}(r)} = \nabla_g^{\mathrm{E}(r)} \boldsymbol{\Theta}_g^{(r)\mathsf{H}} - \boldsymbol{\Theta}_g^{(r)} \nabla_g^{\mathrm{E}(r)\mathsf{H}}; \tag{5}$$

3) Determine the weight factor

$$\gamma_g^{(r)} = \frac{\mathrm{tr}\Big(\big(\nabla_g^{\mathrm{R}(r)} - \nabla_g^{\mathrm{R}(r-1)}\big) \nabla_g^{\mathrm{R}(r)\mathsf{H}}\Big)}{\mathrm{tr}\Big(\nabla_g^{\mathrm{R}(r-1)} \nabla_g^{\mathrm{R}(r-1)\mathsf{H}}\Big)}; \tag{6}$$

4) Compute the conjugate direction

$$\mathbf{D}_g^{(r)} = \nabla_g^{\mathrm{R}(r)} + \gamma_g^{(r)} \mathbf{D}_g^{(r-1)}; \tag{7}$$

5) Determine the Armijo step size[4]

$$\mu_g^{(r)} = \underset{\mu_g}{\mathrm{argmax}} f\Big(\exp\big(\mu_g \mathbf{D}_g^{(r)}\big) \boldsymbol{\Theta}_g^{(r)}\Big); \tag{8}$$

6) Perform rotational update along local geodesics

$$\boldsymbol{\Theta}_g^{(r+1)} = \exp\Big(\mu_g^{(r)} \mathbf{D}_g^{(r)}\Big) \boldsymbol{\Theta}_g^{(r)}. \tag{9}$$

Remark 3. *The adapted RCG method leverages the fact that block unitary matrices are closed under multiplication (but not necessarily under addition). Its advantage over universal manifold optimization [39], [40] is trifold:*

- *No retraction is involved;*
- *Lower computational complexity per iteration [43];*
- *Faster convergence thanks appropriate operational space.*

C. Analytical Bounds

We then analyze the channel shaping *capability* of BD-RIS under specific setups.

1) Rank-Deficient Channel: In rank-deficient channels, BD-RIS $\boldsymbol{\Theta}^{\mathrm{B}}$ cannot achieve a higher Degree of Freedom (DoF) than diagonal RIS $\boldsymbol{\Theta}^{\mathrm{D}}$. This is because $\mathrm{sv}(\boldsymbol{\Theta}^{\mathrm{B}}) = \mathrm{sv}(\boldsymbol{\Theta}^{\mathrm{D}}) = \mathbf{1}$ and

$$\begin{aligned}\mathrm{rank}(\mathbf{H}) &\le \mathrm{rank}(\mathbf{H}^{\mathrm{D}}) + \mathrm{rank}(\mathbf{H}^{\mathrm{B}} \boldsymbol{\Theta} \mathbf{H}^{\mathrm{F}}) \\ &\le \mathrm{rank}(\mathbf{H}^{\mathrm{D}}) + \min\big(\mathrm{rank}(\mathbf{H}^{\mathrm{B}}), \mathrm{rank}(\boldsymbol{\Theta}), \mathrm{rank}(\mathbf{H}^{\mathrm{F}})\big).\end{aligned} \tag{10}$$

Note BD-RIS can still provide a higher indirect Signal-to-Noise Ratio (SNR) as shown in Fig. 4 and 5.

2) Rank-1 Indirect Channel: The indirect channel is rank-1 iff the forward or backward channel is rank-1. Let $\mathbf{H}^{\mathrm{F}} = \sigma^{\mathrm{F}} \mathbf{u}^{\mathrm{F}} \mathbf{v}^{\mathrm{F}\mathsf{H}}$ without loss of generality. In this case, the channel Gram matrix can be written as Hermitian-plus-rank-1:

$$\mathbf{G} \triangleq \mathbf{H}\mathbf{H}^{\mathsf{H}} = \mathbf{Y} + \mathbf{z}\mathbf{z}^{\mathsf{H}}, \tag{11}$$

where $\mathbf{Y} \triangleq \mathbf{H}^{\mathrm{D}}(\mathbf{I} - \mathbf{v}^{\mathrm{F}} \mathbf{v}^{\mathrm{F}\mathsf{H}}) \mathbf{H}^{\mathrm{D}} = \mathbf{T}\mathbf{T}^{\mathsf{H}}$ and $\mathbf{z} \triangleq \sigma^{\mathrm{F}} \mathbf{H}^{\mathrm{B}} \boldsymbol{\Theta} \mathbf{u}^{\mathrm{F}} + \mathbf{H}^{\mathrm{D}} \mathbf{v}^{\mathrm{F}}$. Regardless of RIS size and structure[5], its n-th ($n \ge 2$) eigenvalues are bounded by the Cauchy interlacing formula [46]

$$\lambda_1(\mathbf{Y}) \ge \lambda_2(\mathbf{G}) \ge \lambda_2(\mathbf{Y}) \ge \ldots \ge \lambda_{N-1}(\mathbf{Y}) \ge \lambda_N(\mathbf{G}) \ge \lambda_N(\mathbf{Y}). \tag{12}$$

The equivalent singular value inequality is

$$\sigma_1(\mathbf{T}) \ge \sigma_2(\mathbf{H}) \ge \sigma_2(\mathbf{T}) \ge \ldots \ge \sigma_{N-1}(\mathbf{T}) \ge \sigma_N(\mathbf{H}) \ge \sigma_N(\mathbf{T}). \tag{13}$$

(13) implies that, if the indirect channel is rank-1, then the RIS can at most enlarge the n-th ($n \ge 2$) channel singular value to the $(n-1)$-th singular value of $\mathbf{T}$. Note that the largest channel singular value is unbounded with a sufficiently large RIS.

[4]To double the step size, simply square the argument instead of recomputing the matrix exponential, i.e., $\exp(2\mu_g \mathbf{D}_g) = \exp^2(\mu_g \mathbf{D}_g)$.

[5]A similar conclusion was made for diagonal RIS in [45].

3) Fully-Connected RIS Without Direct Link: Denote the singular value decomposition of forward / backward channels as $\mathbf{H}^{\mathrm{B/F}}=\mathbf{U}^{\mathrm{B/F}}\mathbf{\Sigma}^{\mathrm{B/F}}\mathbf{V}^{\mathrm{B/F}\mathsf{H}}$. The composite channel is

$$\mathbf{H}=\mathbf{H}^{\mathrm{B}}\mathbf{\Theta}\mathbf{H}^{\mathrm{F}}=\mathbf{U}^{\mathrm{B}}\mathbf{\Sigma}^{\mathrm{B}}\mathbf{X}\mathbf{\Sigma}^{\mathrm{F}}\mathbf{V}^{\mathrm{F}\mathsf{H}}, \tag{14}$$

where $\mathbf{X}=\mathbf{V}^{\mathrm{B}\mathsf{H}}\mathbf{\Theta}\mathbf{U}^{\mathrm{F}}$.

Proposition 1. *In this case, the singular value bounds on* $\mathbf{H}$ *are equivalent to the singular value bounds on* $\mathbf{BF}$*, where* $\mathbf{B}$ *and* $\mathbf{F}$ *are arbitrary matrices with singular values* $\mathbf{\Sigma}^{\mathrm{B}}$ *and* $\mathbf{\Sigma}^{\mathrm{F}}$.

Proof. We first observe that singular value control problem can be solved w.r.t. unitary $\mathbf{X}$ and retrieved by $\mathbf{\Theta}=\mathbf{V}^{\mathrm{B}}\mathbf{X}\mathbf{U}^{\mathrm{F}\mathsf{H}}$. Also, $\mathrm{sv}(\mathbf{U}^{\mathrm{B}}\mathbf{\Sigma}^{\mathrm{B}}\mathbf{X}\mathbf{\Sigma}^{\mathrm{F}}\mathbf{V}^{\mathrm{F}\mathsf{H}})=\mathrm{sv}(\bar{\mathbf{U}}^{\mathrm{B}}\mathbf{\Sigma}^{\mathrm{B}}\bar{\mathbf{V}}^{\mathrm{B}\mathsf{H}}\bar{\mathbf{U}}^{\mathrm{F}}\mathbf{\Sigma}^{\mathrm{F}}\bar{\mathbf{V}}^{\mathrm{F}\mathsf{H}})=\mathrm{sv}(\mathbf{BF})$ where $\bar{\mathbf{U}}^{\mathrm{B/F}}$ and $\bar{\mathbf{V}}^{\mathrm{B/F}}$ are arbitrary unitary matrices. □

The problem now becomes, given $\mathbf{\Sigma}^{\mathrm{B}}$ and $\mathbf{\Sigma}^{\mathrm{F}}$, what can we say about the singular value of $\mathbf{BF}$. One comprehensive answer is Horn's inequality [47]: for all admissible triples (I,J,K),

$$\prod_{k\in K}\sigma_k(\mathbf{BF})\le\prod_{i\in I}\sigma_i(\mathbf{B})\prod_{j\in J}\sigma_j(\mathbf{F}). \tag{15}$$

It gives upper bound on the largest singular value and lower bound on the smallest singular value:

$$\sigma_1(\mathbf{BF})\le\sigma_1(\mathbf{B})\sigma_1(\mathbf{F}) \tag{16}$$

$$\sigma_N(\mathbf{BF})\ge\sigma_N(\mathbf{B})\sigma_N(\mathbf{F}). \tag{17}$$

Another useful result is introduced in [48]: for all $p>0$,

$$\sum_n\sigma_n^p(\mathbf{BF})\le\sum_n\sigma_n^p(\mathbf{B})\sigma_n^p(\mathbf{F}). \tag{18}$$

When $p=2$, it implies the channel energy is upper bounded by the sum of element-wise power product of the forward and backward channels, as illustrated in Fig. 5(a). Interestingly, (16)–(18) are simultaneously tight when $\mathbf{X}=\mathbf{I}$ and $\mathbf{\Theta}=\mathbf{V}^{\mathrm{B}}\mathbf{U}^{\mathrm{F}\mathsf{H}}$. This solution was claimed in [27] to achieve channel capacity, but it is not true at moderate SNR.

Finally, we characterize the *Pareto frontier* of channel singular values via optimization approach.

where ρ_n is the weight of n-th singular value. The complex derivative of (3a) w.r.t. RIS block g is

$$\frac{\partial J_1}{\partial\mathbf{\Theta}_g^*}=\mathbf{H}_g^{\mathrm{B}\mathsf{H}}\mathbf{U}\mathrm{diag}(\boldsymbol{\rho})\mathbf{V}^{\mathsf{H}}\mathbf{H}_g^{\mathrm{F}\mathsf{H}}, \tag{19}$$

where $\mathbf{U}$ and $\mathbf{V}$ are left and right singular matrix of $\mathbf{H}$. (3) can be solved by RCG Algorithm 2 with (27) replaced by (19).

The Pareto frontier and evolving trend of channel singular values are shown in Fig. 2 and 3. Clearly, BD-RIS with a larger group size can redistribute the channel singular values to a wider range.

D. Channel Power Maximization

Consider a BD-RIS with N^{S} elements, which is divided into G groups of equal L elements.

$$\max_{\mathbf{\Theta}}\quad\left\|\mathbf{H}^{\mathrm{D}}+\sum\nolimits_g\mathbf{H}_g^{\mathrm{B}}\mathbf{\Theta}_g\mathbf{H}_g^{\mathrm{F}}\right\|_{\mathrm{F}}^2 \tag{20a}$$

$$\text{s.t.}\quad\mathbf{\Theta}_g^{\mathsf{H}}\mathbf{\Theta}_g=\mathbf{I},\quad\forall g\in\mathcal{G}\triangleq\{1,\ldots,G\}. \tag{20b}$$

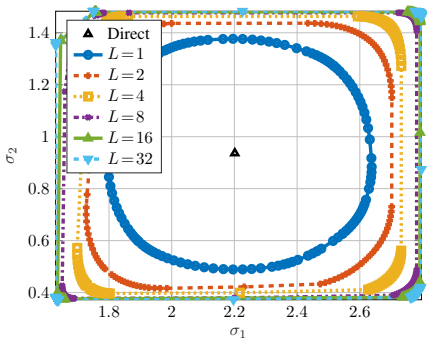

Fig. 2. Singular value Pareto frontier. $(N^{\mathrm{T}},N^{\mathrm{S}},N^{\mathrm{R}})=(4,64,2)$, $(\Lambda^{\mathrm{D}},\Lambda^{\mathrm{F}},\Lambda^{\mathrm{B}})=(0,-17.5,-17.5)$dB.

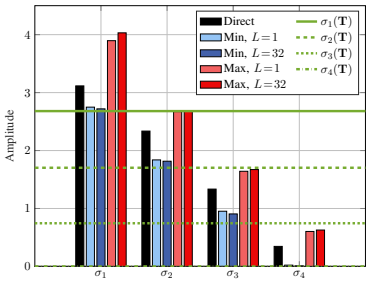

Fig. 3. Singular value bounds for rank-1 indirect channel. $(N^{\mathrm{T}},N^{\mathrm{S}},N^{\mathrm{R}})=(4,32,4)$, $(\Lambda^{\mathrm{D}},\Lambda^{\mathrm{F}},\Lambda^{\mathrm{B}})=(0,-17.5,-17.5)$dB.

For *symmetric* BD-RIS, the problem has been solved in

- Matteo's paper [21]: SISO and equivalent[6];
- Ignacio's paper [22]: SISO and directless MISO/SIMO.

Remark 4. *The difficulty of* (20) *is that the RIS needs to balance the additive (direct-indirect) and multiplicative (forward-backward) eigenspace alignment. Interestingly, it has the same form as the* weighted orthogonal Procrustes problem *[49]:*

$$\min_{\mathbf{\Theta}}\quad\|\mathbf{C}-\mathbf{A}\mathbf{\Theta}\mathbf{B}\|_{\mathrm{F}}^2 \tag{21a}$$

$$\text{s.t.}\quad\mathbf{\Theta}^{\mathsf{H}}\mathbf{\Theta}=\mathbf{I}. \tag{21b}$$

There exists no trivial solution to (21)*. One lossy transformation, by moving* $\mathbf{\Theta}$ *to one side [50], formulates a standard orthogonal Procrustes problem:*

$$\min_{\mathbf{\Theta}}\quad\|\mathbf{A}^{\dagger}\mathbf{C}-\mathbf{\Theta}\mathbf{B}\|_{\mathrm{F}}^2 \tag{22a}$$

$$\text{s.t.}\quad\mathbf{\Theta}^{\mathsf{H}}\mathbf{\Theta}=\mathbf{I}. \tag{22b}$$

(22) *has a global optimal solution* $\mathbf{\Theta}^{\star}=\mathbf{U}\mathbf{V}^{\mathsf{H}}$*, where* $\mathbf{U}$ *and* $\mathbf{V}$ *are left and right singular matrix of* $\mathbf{A}^{\dagger}\mathbf{C}\mathbf{B}^{\mathsf{H}}$ *[46]. This low-complexity solution will be compared with the one proposed later.*

Inspired by [51], we propose an iterative algorithm to solve (20). The idea is to successively approximate the quadratic objective with a sequence of affine functions and solve the resulting subproblems in closed form.

[6]Single-stream MIMO with given precoder and combiner.

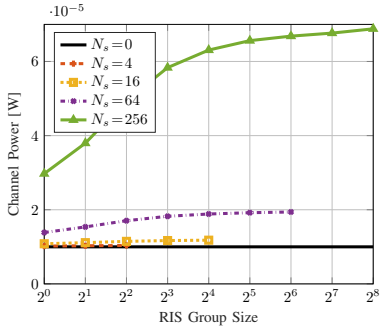

Fig. 4. Average channel power versus RIS elements N^{S} and group size L. $(N^{\mathrm{T}},N^{\mathrm{R}})=(8,4)$, $(\Lambda^{\mathrm{D}},\Lambda^{\mathrm{F}},\Lambda^{\mathrm{B}})=(65,54,46)$dB.

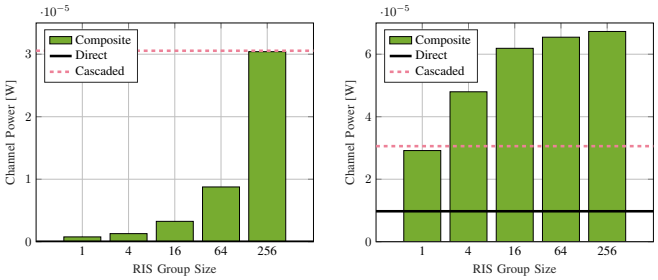

(a) Without Direct Link (b) With Direct Link

Fig. 5. Average channel power versus RIS group size L. $(N^{\mathrm{T}},N^{\mathrm{S}},N^{\mathrm{R}})=(8,256,4)$, $(\Lambda^{\mathrm{D}},\Lambda^{\mathrm{F}},\Lambda^{\mathrm{B}})=(65,54,46)$dB.

Proposition 2. *Start from any* $\boldsymbol{\Theta}^{(0)}$*, the sequence*

$$\boldsymbol{\Theta}_g^{(r+1)}=\mathbf{U}_g^{(r)}\mathbf{V}_g^{(r)},\quad \forall g \tag{23}$$

converges to a stationary point of (20)*, where* $\mathbf{U}_g^{(r)}$ *and* $\mathbf{V}_g^{(r)}$ *are left and right singular matrix of*

$$\begin{aligned}\mathbf{M}_g^{(r)}=&\mathbf{H}_g^{\mathrm{B}}{}^{\mathsf{H}}\mathbf{H}^{\mathrm{D}}\mathbf{H}_g^{\mathrm{F}}{}^{\mathsf{H}}+\sum_{g'<g}\mathbf{H}_{g'}^{\mathrm{B}}{}^{\mathsf{H}}\mathbf{H}_{g'}^{\mathrm{B}}\boldsymbol{\Theta}_{g'}^{(r+1)}\mathbf{H}_{g'}^{\mathrm{F}}\mathbf{H}_{g'}^{\mathrm{F}}{}^{\mathsf{H}}\\&+\sum_{g'\geq g}\mathbf{H}_{g'}^{\mathrm{B}}{}^{\mathsf{H}}\mathbf{H}_{g'}^{\mathrm{B}}\boldsymbol{\Theta}_{g'}^{(r)}\mathbf{H}_{g'}^{\mathrm{F}}\mathbf{H}_{g'}^{\mathrm{F}}{}^{\mathsf{H}}.\end{aligned} \tag{24}$$

Proof. To be added. □

Fig. 4 shows that, apart from adding reflecting elements N^{S}, increasing the group size L also improves the channel power. This behavior is more pronounced for a large RIS. For example, the gain of pairwise connection is $2.8\,\%$ for $N^{\mathrm{S}}=16$ and $28\,\%$ for $N^{\mathrm{S}}=256$. It implies that the channel shaping capability of BD-RIS scales with group size L.

Fig. 5b and 5a compare the average channel power without and with direct link. "Cascaded" means the sum of element-wise product of first $N=\min(N^{\mathrm{T}},N^{\mathrm{S}},N^{\mathrm{R}})$ eigenvalues (i.e., element-wise power product) of the forward and backward channels. We observe that diagonal RIS wastes substantial cascaded power and struggles to align the direct-indirect eigenspace. When the direct link is absent, only $2.6\,\%$ of available power is utilized by diagonal RIS while $100\,\%$ power is recycled by fully-connected RIS. When the direct link is present, the proposed BD-RIS design can balance the direct-indirect and forward-backward eigenspace alignment for an optimal channel boost. It is worth noting that, when L is sufficiently large, the composite channel power surpasses the power sum of direct and cascaded channels, thanks to the constructive *amplitude superposition* of direct and cascaded channels. This again emphasizes the advantage of in-group connection of BD-RIS.

Algorithm 2: RCG Method for RIS MIMO-Point-to-point Channel (PC) Rate Maximization

Input: $\mathbf{H}^{\mathrm{D}}$, $\mathbf{H}^{\mathrm{F}}$, $\mathbf{H}^{\mathrm{B}}$, $\mathbf{W}$, L, η
Output: $\boldsymbol{\Theta}^{\star}$
1: $r\leftarrow 0$, $\boldsymbol{\Theta}^{(0)}$
2: **Repeat**
3: $r\leftarrow r+1$
4: **For** $g\leftarrow 1$ to G
5: $\boldsymbol{\Theta}_g^{(r)}\leftarrow$ (27), (5)–(9)
6: **End For**
7: **Until** $|R^{(r)}-R^{(r-1)}|/R^{(r-1)}\leq\epsilon$

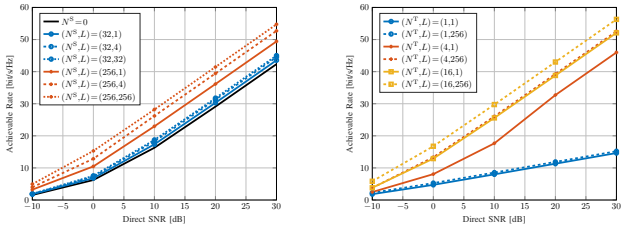

(a) RIS Elements, $N^{\mathrm{T}}=8$ (b) Transmit Antenna, $N^{\mathrm{S}}=256$

Fig. 6. Average achievable rate versus group size L. $N^{\mathrm{R}}=4$, $(\Lambda^{\mathrm{D}},\Lambda^{\mathrm{F}},\Lambda^{\mathrm{B}})=(65,54,46)$dB.

E. Rate Maximization

The problem is formulated w.r.t. precoder (instead of transmit covariance matrix) for reference:

$$\max_{\mathbf{W},\boldsymbol{\Theta}}\quad R=\log\det\left(\mathbf{I}+\frac{\mathbf{W}^{\mathsf{H}}\mathbf{H}^{\mathsf{H}}\mathbf{H}\mathbf{W}}{\eta}\right) \tag{25a}$$

$$\text{s.t.}\quad \|\mathbf{W}\|_{\mathrm{F}}^2\leq P, \tag{25b}$$

$$\boldsymbol{\Theta}_g^{\mathsf{H}}\boldsymbol{\Theta}_g=\mathbf{I},\quad\forall g. \tag{25c}$$

(25) is jointly non-convex and solved by AO. For a given $\boldsymbol{\Theta}$, the optimal precoder is given by

$$\mathbf{W}^{\star}=\mathbf{V}\mathbf{S}^{\star 1/2}, \tag{26}$$

where $\mathbf{V}$ is right singular matrix of $\mathbf{H}$ and $\mathbf{S}^{\star}$ is a diagonal matrix of the water-filling power allocation. For a given $\mathbf{W}$, The complex derivative of (25a) w.r.t. RIS block g is

$$\frac{\partial R}{\partial\boldsymbol{\Theta}_g^{*}}=\frac{1}{\eta}\mathbf{H}_g^{\mathrm{B}}{}^{\mathsf{H}}\mathbf{H}\mathbf{W}\left(\mathbf{I}+\frac{\mathbf{W}^{\mathsf{H}}\mathbf{H}^{\mathsf{H}}\mathbf{H}\mathbf{W}}{\eta}\right)^{-1}\mathbf{W}^{\mathsf{H}}\mathbf{H}_g^{\mathrm{F}}{}^{\mathsf{H}}. \tag{27}$$

Algorithm 2 summarizes the adapted RCG method for the RIS rate maximization subproblem.

Fig. 6a illustrates how RIS configuration influences the MIMO PC achievable rate. To ensure a $20\,\mathrm{bit/s/Hz}$ transmission, an SNR of $13.5\,\mathrm{dB}$ is required for a 8T4R system. This value decreases to $12.5\,\mathrm{dB}$ (resp. $8\,\mathrm{dB}$) when 32- (resp. 256-) element diagonal RIS is present. If tetrads can be formed in BD-RIS, the SNR can be reduced by another $20\,\%$ (resp.

44 %). Further increase in L yields a marginal gain and incurs $\mathcal{O}(L^2)$ connections. We thus conclude dyadic or tetradic BD-RIS usually strike a good balance between performance and complexity.

IV. MIMO-IC

A. Leakage Interference Minimization

$$\min_{\boldsymbol{\Theta},\{\mathbf{G}_k\},\{\mathbf{W}_k\}} \quad \sum_{j\neq k}\sum \left\|\mathbf{G}_k(\mathbf{H}_{kj}^{\mathrm{D}}+\mathbf{H}_k^{\mathrm{B}}\boldsymbol{\Theta}\mathbf{H}_j^{\mathrm{F}})\mathbf{W}_j\right\|_{\mathrm{F}}^2 \tag{28a}$$

$$\text{s.t.} \quad \boldsymbol{\Theta}_g^{\mathsf{H}}\boldsymbol{\Theta}_g=\mathbf{I}, \quad \forall g, \tag{28b}$$

$$\mathbf{G}_k\mathbf{G}_k^{\mathsf{H}}=\mathbf{I}, \quad \mathbf{W}_k^{\mathsf{H}}\mathbf{W}_k=\mathbf{I}, \quad \forall k. \tag{28c}$$

The non-convex problem can be solved by Block Coordinate Descent (BCD) method. For a given $\boldsymbol{\Theta}$, it reduces to conventional linear beamforming problem, for which an iterative algorithm alternating between the original and reciprocal networks is proposed in [52], [53]. At iteration r, the combiner at receiver k is updated as

$$\mathbf{G}_k^{(r)}=\mathbf{U}_{k,N}^{(r-1)^{\mathsf{H}}}, \tag{29}$$

where $\mathbf{U}_{k,N}^{(r-1)}$ is the eigenvectors corresponding to N smallest eigenvalues of interference covariance matrix $\mathbf{Q}_k^{(r-1)}=\sum_{j\neq k}\mathbf{H}_{kj}\mathbf{W}_j^{(r-1)}\mathbf{W}_j^{(r-1)^{\mathsf{H}}}\mathbf{H}_{kj}^{\mathsf{H}}$. The precoder at transmitter j is updated as

$$\mathbf{W}_j^{(r)}=\bar{\mathbf{U}}_{j,N}^{(r)}, \tag{30}$$

where $\bar{\mathbf{U}}_{j,N}^{(r)}$ corresponds to interference covariance matrix $\bar{\mathbf{Q}}_j^{(r)}=\sum_{k\neq j}\mathbf{H}_{kj}^{\mathsf{H}}\mathbf{G}_k^{(r)^{\mathsf{H}}}\mathbf{G}_k^{(r)}\mathbf{H}_{kj}$ in the reciprocal network. Once $\{\mathbf{G}_k\}$ and $\{\mathbf{W}_k\}$ are determined, we define $\bar{\mathbf{H}}_{kj}^{\mathrm{D}}\triangleq\mathbf{G}_k\mathbf{H}_{kj}^{\mathrm{D}}\mathbf{W}_j$, $\bar{\mathbf{H}}_k^{\mathrm{B}}\triangleq\mathbf{G}_k\mathbf{H}_k^{\mathrm{B}}$, and $\bar{\mathbf{H}}_j^{\mathrm{F}}\triangleq\mathbf{H}_j^{\mathrm{F}}\mathbf{W}_j$. The BD-RIS subproblem reduces to

$$\min_{\boldsymbol{\Theta}} \quad \sum_{j\neq k}\sum \left\|(\bar{\mathbf{H}}_{kj}^{\mathrm{D}}+\bar{\mathbf{H}}_k^{\mathrm{B}}\boldsymbol{\Theta}\bar{\mathbf{H}}_j^{\mathrm{F}})\right\|_{\mathrm{F}}^2 \tag{31a}$$

$$\text{s.t.} \quad \boldsymbol{\Theta}_g^{\mathsf{H}}\boldsymbol{\Theta}_g=\mathbf{I}, \quad \forall g. \tag{31b}$$

Proposition 3. *Start from any $\boldsymbol{\Theta}^{(0)}$, the sequence*

$$\boldsymbol{\Theta}_g^{(r+1)}=\mathbf{U}_g^{(r)}\mathbf{V}_g^{(r)}, \quad \forall g \tag{32}$$

converges to a stationary point of (31)*, where $\mathbf{U}_g^{(r)}$ and $\mathbf{V}_g^{(r)}$ are left and right singular matrix of*

$$\mathbf{M}_g^{(r)}=\sum_{j\neq k}\sum\left(\mathbf{B}_{k,g}\boldsymbol{\Theta}_g^{(r)}\mathbf{H}_{j,g}^{\mathrm{F}}-\mathbf{H}_{k,g}^{\mathrm{B}\ \mathsf{H}}\mathbf{D}_{kj,g}^{(r)}\right)\mathbf{H}_{j,g}^{\mathrm{F}\ \mathsf{H}}, \tag{33}$$

where $\mathbf{B}_{k,g}=\lambda_1\left(\mathbf{H}_{k,g}^{\mathrm{B}}\mathbf{H}_{k,g}^{\mathrm{B}\ \mathsf{H}}\right)\mathbf{I}-\mathbf{H}_{k,g}^{\mathrm{B}\ \mathsf{H}}\mathbf{H}_{k,g}^{\mathrm{B}}$ *and*

$$\mathbf{D}_{kj,g}^{(r)}=\mathbf{H}_{jk}^{\mathrm{D}}+\sum_{g'<g}\mathbf{H}_{k,g'}^{\mathrm{B}\ \mathsf{H}}\boldsymbol{\Theta}_{g'}^{(r+1)}\mathbf{H}_{k,g'}^{\mathrm{F}}+\sum_{g'>g}\mathbf{H}_{k,g'}^{\mathrm{B}\ \mathsf{H}}\boldsymbol{\Theta}_{g'}^{(r)}\mathbf{H}_{k,g'}^{\mathrm{F}}. \tag{34}$$

Proof. To be added. □

Fig. 7 illustrates how BD-RIS helps to reduce the leakage interference. In this case, a fully-connected 2^n-element BD-RIS is almost as good as a diagonal 2^{n+2}-element RIS in terms of leakage interference. Interestingly, the result suggests

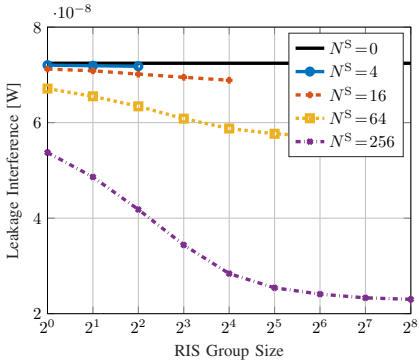

Fig. 7. Average leakage interference versus RIS elements N^{S} and group size L. Transmitters and receivers are randomly generated in a disk of radius 50 m centered at the RIS. $(N^{\mathrm{T}},N^{\mathrm{R}},N^{\mathrm{E}},K)=(8,4,3,5)$, $(\gamma^{\mathrm{D}},\gamma^{\mathrm{F}},\gamma^{\mathrm{B}})=(3,2.4,2.4)$, and reference pathloss at 1 m is -30 dB.

that BD-RIS can achieve a higher DoF than diagonal RIS in MIMO-Interference Channel (IC), which is not the case in MIMO-PC (as discussed in III-C1).

B. Weighted Sum-Rate Maximization

$$\max_{\boldsymbol{\Theta},\{\mathbf{W}_k\}} \quad J_2=\sum_k \rho_k \mathrm{logdet}\left(\mathbf{I}+\mathbf{W}_k\mathbf{H}_{kj}^{\mathsf{H}}\mathbf{Q}_k^{-1}\mathbf{H}_{kj}\mathbf{W}_k\right) \tag{35a}$$

$$\text{s.t.} \quad \boldsymbol{\Theta}_g^{\mathsf{H}}\boldsymbol{\Theta}_g=\mathbf{I}, \quad \forall g, \tag{35b}$$

$$\|\mathbf{W}_k\|_{\mathrm{F}}^2\leq P_k. \quad \forall k \tag{35c}$$

where ρ_k is the weight of user k and $\mathbf{Q}_k$ is the interference-plus-noise covariance matrix

$$\mathbf{Q}_k=\sum_{j\neq k}\mathbf{H}_{kj}\mathbf{W}_j\mathbf{W}_j^{\mathsf{H}}\mathbf{H}_{kj}^{\mathsf{H}}+\eta\mathbf{I}. \tag{36}$$

For a given $\boldsymbol{\Theta}$, (35) reduces to conventional linear beamforming problem, for which a closed-form iterative solution based on Weighted Sum-Rate (WSR)-Weighted MMSE (WMMSE) relationship is proposed in [54]. At iteration r, the Minimum Mean-Square Error (MMSE) combiner at receiver k is

$$\mathbf{G}_k^{(r)}=\mathbf{W}_k^{(r-1)^{\mathsf{H}}}\mathbf{H}_{kk}^{\mathsf{H}}\left(\mathbf{Q}_k^{(r-1)}+\mathbf{H}_{kk}\mathbf{W}_k^{(r-1)}\mathbf{W}_k^{(r-1)^{\mathsf{H}}}\mathbf{H}_{kk}^{\mathsf{H}}\right)^{-1}, \tag{37}$$

the corresponding error matrix is

$$\mathbf{E}_k^{(r)}=\left(\mathbf{I}+\mathbf{W}_k^{(r-1)^{\mathsf{H}}}\mathbf{H}_{kk}^{\mathsf{H}}\mathbf{Q}_k^{(r-1)}\mathbf{H}_{kk}\mathbf{W}_k^{(r-1)}\right)^{-1}, \tag{38}$$

the Mean-Square Error (MSE) weight is

$$\boldsymbol{\Omega}_k^{(r)}=\rho_k\mathbf{E}_k^{(r)^{-1}}, \tag{39}$$

the Lagrange multiplier is

$$\lambda_k^{(r)}=\frac{\mathrm{tr}\left(\eta\boldsymbol{\Omega}_k^{(r)}\mathbf{G}_k^{(r)}\mathbf{G}_k^{(r)^{\mathsf{H}}}+\sum_j\boldsymbol{\Omega}_k^{(r)}\mathbf{T}_{kj}^{(r)}\mathbf{T}_{kj}^{(r)^{\mathsf{H}}}-\boldsymbol{\Omega}_j^{(r)}\mathbf{T}_{jk}^{(r)}\mathbf{T}_{jk}^{(r)^{\mathsf{H}}}\right)}{P_k}, \tag{40}$$

where $\mathbf{T}_{kj}^{(r)}=\mathbf{G}_k^{(r)}\mathbf{H}_{kj}\mathbf{W}_j^{(r)}$. The precoder at transmitter k is

$$\mathbf{W}_k^{(r)}=\left(\sum_j\mathbf{H}_{jk}^{\mathsf{H}}\mathbf{G}_j^{(r)^{\mathsf{H}}}\boldsymbol{\Omega}_k^{(r)}\mathbf{G}_j^{(r)}\mathbf{H}_{jk}+\lambda_k^{(r)}\mathbf{I}\right)^{-1}\mathbf{H}_{kk}^{\mathsf{H}}\mathbf{G}_j^{(r)^{\mathsf{H}}}\boldsymbol{\Omega}_k^{(r)}. \tag{41}$$

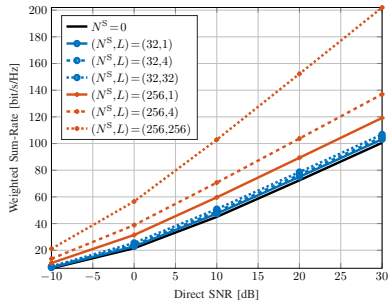

Fig. 8. Average weighted sum-rate versus SNR, RIS elements N^{S} and group size L. $(N^{\mathrm{T}},N^{\mathrm{R}},N^{\mathrm{E}},K)=(8,4,3,5)$, $(\Lambda^{\mathrm{D}},\Lambda^{\mathrm{F}},\Lambda^{\mathrm{B}})=(65,54,46)$dB, $\rho_k=1$, $\forall k$.

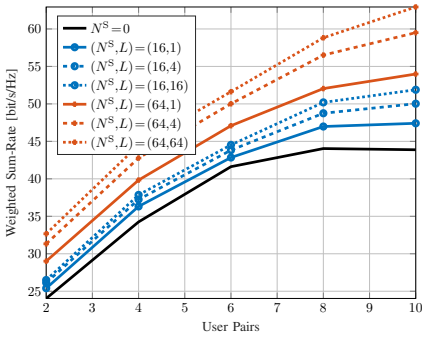

Fig. 9. Average weighted sum-rate versus user pairs K, RIS elements N^{S} and group size L at $\mathrm{SNR}=15$dB. $(N^{\mathrm{T}},N^{\mathrm{R}},N^{\mathrm{E}})=(4,4,3)$, $\rho_k=1$, $\forall k$.

Once $\{\mathbf{W}_k\}$ is determined, the complex derivative of (35a) w.r.t. RIS block g is

$$\frac{\partial J_2}{\partial \boldsymbol{\Theta}_g^*}=\sum_k \rho_k \mathbf{H}_{k,g}^{\mathrm{B}\ \mathsf{H}}\mathbf{Q}_k^{-1}\mathbf{H}_{kk}\mathbf{W}_k\mathbf{E}_k\mathbf{W}_k^{\mathsf{H}} \times\left(\mathbf{H}_{k,g}^{\mathrm{F}\ \mathsf{H}}-\mathbf{H}_{kk}^{\mathsf{H}}\mathbf{Q}_k^{-1}\sum_{j\neq k}\mathbf{H}_{kj}\mathbf{W}_j\mathbf{W}_j^{\mathsf{H}}\mathbf{H}_{j,g}^{\mathrm{F}\ \mathsf{H}}\right). \tag{42}$$

The RIS subproblem can be solved by RCG Algorithm 2 with (27) replaced by (42).

A new observation from Fig. 8 that the interference alignment capability of BD-RIS scales much faster with group size than number of elements.[7]

REFERENCES

[1] E. Basar, M. D. Renzo, J. D. Rosny, M. Debbah, M.-S. Alouini, and R. Zhang, "Wireless communications through reconfigurable intelligent surfaces," *IEEE Access*, vol. 7, pp. 116 753–116 773, 2019. [Online]. Available: https://ieeexplore.ieee.org/document/8796365/

[2] Q. Wu and R. Zhang, "Intelligent reflecting surface enhanced wireless network via joint active and passive beamforming," *IEEE Transactions on Wireless Communications*, vol. 18, pp. 5394–5409, 11 2019. [Online]. Available: https://ieeexplore.ieee.org/document/8811733/

[3] ——, "Beamforming optimization for wireless network aided by intelligent reflecting surface with discrete phase shifts," *IEEE Transactions on Communications*, vol. 68, pp. 1838–1851, 3 2020. [Online]. Available: https://ieeexplore.ieee.org/document/8930608/

[4] Y. Yang, S. Zhang, and R. Zhang, "Irs-enhanced ofdma: Joint resource allocation and passive beamforming optimization," *IEEE Wireless Communications Letters*, vol. 9, pp. 760–764, 6 2020. [Online]. Available: https://ieeexplore.ieee.org/document/8964457/

[7]The results are not very stable and depend heavily on initialization.

[5] B. Zheng, C. You, and R. Zhang, "Double-irs assisted multi-user mimo: Cooperative passive beamforming design," *IEEE Transactions on Wireless Communications*, vol. 20, pp. 4513–4526, 7 2021. [Online]. Available: https://ieeexplore.ieee.org/document/9362274/

[6] X. Jia, J. Zhao, X. Zhou, and D. Niyato, "Intelligent reflecting surface-aided backscatter communications," vol. 2020-Janua. IEEE, 12 2020, pp. 1–6. [Online]. Available: https://ieeexplore.ieee.org/document/9348003/

[7] Y. C. Liang, Q. Zhang, J. Wang, R. Long, H. Zhou, and G. Yang, "Backscatter communication assisted by reconfigurable intelligent surfaces," *Proceedings of the IEEE*, 2022.

[8] R. Liu, M. Li, Y. Liu, Q. Wu, and Q. Liu, "Joint transmit waveform and passive beamforming design for ris-aided dfrc systems," *IEEE Journal of Selected Topics in Signal Processing*, pp. 1–1, 5 2022.

[9] M. Hua, Q. Wu, C. He, S. Ma, and W. Chen, "Joint active and passive beamforming design for irs-aided radar-communication," *IEEE Transactions on Wireless Communications*, vol. 22, pp. 2278–2294, 4 2023.

[10] Q. Wu, X. Zhou, W. Chen, J. Li, and X. Zhang, "Irs-aided wpcns: A new optimization framework for dynamic irs beamforming," *IEEE Transactions on Wireless Communications*, pp. 1–1, 12 2021.

[11] Z. Feng, B. Clerckx, and Y. Zhao, "Waveform and beamforming design for intelligent reflecting surface aided wireless power transfer: Single-user and multi-user solutions," *IEEE Transactions on Wireless Communications*, 2022.

[12] Y. Zhao, B. Clerckx, and Z. Feng, "Irs-aided swipt: Joint waveform, active and passive beamforming design under nonlinear harvester model," *IEEE Transactions on Communications*, vol. 70, pp. 1345–1359, 2022.

[13] R. Karasik, O. Simeone, M. D. Renzo, and S. S. Shitz, "Beyond max-snr: Joint encoding for reconfigurable intelligent surfaces," vol. 2020-June. IEEE, 6 2020, pp. 2965–2970. [Online]. Available: https://ieeexplore.ieee.org/document/9174060/

[14] E. Basar, "Reconfigurable intelligent surface-based index modulation: A new beyond mimo paradigm for 6g," *IEEE Transactions on Communications*, vol. 68, pp. 3187–3196, 5 2020. [Online]. Available: https://ieeexplore.ieee.org/document/8981888/

[15] Y. Zhao and B. Clerckx, "Riscatter: Unifying backscatter communication and reconfigurable intelligent surface," 12 2022. [Online]. Available: http://arxiv.org/abs/2212.09121

[16] W. Tang, J. Y. Dai, M. Chen, X. Li, Q. Cheng, S. Jin, K. Wong, and T. J. Cui, "Programmable metasurface-based rf chain-free 8psk wireless transmitter," *Electronics Letters*, vol. 55, pp. 417–420, 4 2019. [Online]. Available: https://onlinelibrary.wiley.com/doi/10.1049/el.2019.0400

[17] J. Y. Dai, W. Tang, L. X. Yang, X. Li, M. Z. Chen, J. C. Ke, Q. Cheng, S. Jin, and T. J. Cui, "Realization of multi-modulation schemes for wireless communication by time-domain digital coding metasurface," *IEEE Transactions on Antennas and Propagation*, vol. 68, pp. 1618–1627, 3 2020. [Online]. Available: https://ieeexplore.ieee.org/document/8901437/

[18] Q. Wu and R. Zhang, "Towards smart and reconfigurable environment: Intelligent reflecting surface aided wireless network," *IEEE Communications Magazine*, vol. 58, pp. 106–112, 1 2020. [Online]. Available: https://ieeexplore.ieee.org/document/8910627/

[19] S. Shen, B. Clerckx, and R. Murch, "Modeling and architecture design of reconfigurable intelligent surfaces using scattering parameter network analysis," *IEEE Transactions on Wireless Communications*, pp. 1–1, 11 2021. [Online]. Available: https://ieeexplore.ieee.org/document/9514409/

[20] H. Li, S. Shen, and B. Clerckx, "Beyond diagonal reconfigurable intelligent surfaces: From transmitting and reflecting modes to single-, group-, and fully-connected architectures," *IEEE Transactions on Wireless Communications*, vol. 22, pp. 2311–2324, 4 2023.

[21] M. Nerini, S. Shen, and B. Clerckx, "Closed-form global optimization of beyond diagonal reconfigurable intelligent surfaces," *IEEE Transactions on Wireless Communications*, pp. 1–1, 2023. [Online]. Available: https://ieeexplore.ieee.org/document/10155675/

[22] I. Santamaria, M. Soleymani, E. Jorswieck, and J. Gutiérrez, "Snr maximization in beyond diagonal ris-assisted single and multiple antenna links," *IEEE Signal Processing Letters*, vol. 30, pp. 923–926, 2023. [Online]. Available: https://ieeexplore.ieee.org/document/10187688/

[23] T. Fang and Y. Mao, "A low-complexity beamforming design for beyond-diagonal ris aided multi-user networks," *IEEE Communications Letters*, pp. 1–1, 7 2023. [Online]. Available: https://ieeexplore.ieee.org/document/10319662/

[24] M. Nerini, S. Shen, H. Li, and B. Clerckx, "Beyond diagonal reconfigurable intelligent surfaces utilizing graph theory: Modeling, architecture design, and optimization," 5 2023. [Online]. Available: http://arxiv.org/abs/2305.05013

[25] Y. Zhou, Y. Liu, H. Li, Q. Wu, S. Shen, and B. Clerckx, "Optimizing power consumption, energy efficiency and sum-rate using beyond diagonal ris — a unified approach," *IEEE Transactions*

on Wireless Communications, pp. 1–1, 2023. [Online]. Available: https://ieeexplore.ieee.org/document/10364738/

[26] H. Li, S. Shen, and B. Clerckx, "A dynamic grouping strategy for beyond diagonal reconfigurable intelligent surfaces with hybrid transmitting and reflecting mode," *IEEE Transactions on Vehicular Technology*, 12 2023.

[27] G. Bartoli, A. Abrardo, N. Decarli, D. Dardari, and M. D. Renzo, "Spatial multiplexing in near field mimo channels with reconfigurable intelligent surfaces," *IET Signal Processing*, vol. 17, 3 2023. [Online]. Available: https://ietresearch.onlinelibrary.wiley.com/doi/10.1049/sil2.12195

[28] H. Li, S. Shen, and B. Clerckx, "Beyond diagonal reconfigurable intelligent surfaces: A multi-sector mode enabling highly directional full-space wireless coverage," *IEEE Journal on Selected Areas in Communications*, vol. 41, pp. 2446–2460, 8 2023.

[29] H. Li, Y. Zhang, and B. Clerckx, "Channel estimation for beyond diagonal reconfigurable intelligent surfaces with group-connected architectures," 7 2023. [Online]. Available: http://arxiv.org/abs/2307.06129

[30] H. Li, S. Shen, M. Nerini, M. D. Renzo, and B. Clerckx, "Beyond diagonal reconfigurable intelligent surfaces with mutual coupling: Modeling and optimization," 10 2023. [Online]. Available: http://arxiv.org/abs/2310.02708

[31] H. Li, S. Shen, M. Nerini, and B. Clerckx, "Reconfigurable intelligent surfaces 2.0: Beyond diagonal phase shift matrices," 1 2023. [Online]. Available: http://arxiv.org/abs/2301.03288

[32] B. Ning, Z. Chen, W. Chen, and J. Fang, "Beamforming optimization for intelligent reflecting surface assisted mimo: A sum-path-gain maximization approach," *IEEE Wireless Communications Letters*, vol. 9, pp. 1105–1109, 7 2020.

[33] O. Ozdogan, E. Bjornson, and E. G. Larsson, "Using intelligent reflecting surfaces for rank improvement in mimo communications." IEEE, 5 2020, pp. 9160–9164. [Online]. Available: https://ieeexplore.ieee.org/document/9052904/

[34] G.-H. Li, D.-W. Yue, and S.-N. Jin, "Spatially correlated rayleigh fading characteristics of ris-aided mmwave mimo communications," *IEEE Communications Letters*, vol. 27, pp. 2222–2226, 8 2023. [Online]. Available: https://ieeexplore.ieee.org/document/10164200/

[35] Y. Zheng, T. Lin, and Y. Zhu, "Passive beamforming for irs-assisted mu-mimo systems with one-bit adcs: An ser minimization design approach," *IEEE Communications Letters*, vol. 26, pp. 1101–1105, 5 2022. [Online]. Available: https://ieeexplore.ieee.org/document/9706177/

[36] W. Huang, B. Lei, S. He, C. Kai, and C. Li, "Condition number improvement of irs-aided near-field mimo channels." IEEE, 5 2023, pp. 1210–1215. [Online]. Available: https://ieeexplore.ieee.org/document/10283534/

[37] M. A. ElMossallamy, H. Zhang, R. Sultan, K. G. Seddik, L. Song, G. Y. Li, and Z. Han, "On spatial multiplexing using reconfigurable intelligent surfaces," *IEEE Wireless Communications Letters*, vol. 10, pp. 226–230, 2 2021. [Online]. Available: https://ieeexplore.ieee.org/document/9200661/

[38] S. Meng, W. Tang, W. Chen, J. Lan, Q. Y. Zhou, Y. Han, X. Li, and S. Jin, "Rank optimization for mimo channel with ris: Simulation and measurement," 7 2023. [Online]. Available: http://arxiv.org/abs/2307.13237

[39] P.-A. Absil, R. Mahony, and R. Sepulchre, *Optimization Algorithms on Matrix Manifolds*. Princeton University Press, 2009. [Online]. Available: https://books.google.co.uk/books?id=NSQGQeLN3NcC

[40] C. Pan, G. Zhou, K. Zhi, S. Hong, T. Wu, Y. Pan, H. Ren, M. D. Renzo, A. L. Swindlehurst, R. Zhang, and A. Y. Zhang, "An overview of signal processing techniques for ris/irs-aided wireless systems," *IEEE Journal of Selected Topics in Signal Processing*, vol. 16, pp. 883–917, 8 2022. [Online]. Available: https://ieeexplore.ieee.org/document/9847080/

[41] M. T. Ivrlac and J. A. Nossek, "Toward a circuit theory of communication," *IEEE Transactions on Circuits and Systems I: Regular Papers*, vol. 57, pp. 1663–1683, 7 2010. [Online]. Available: https://ieeexplore.ieee.org/document/5446312/

[42] H.-R. Ahn, *Asymmetric Passive Components in Microwave Integrated Circuits*. Wiley, 2006. [Online]. Available: https://books.google.co.uk/books?id=X6WdLbOuSNQC

[43] T. E. Abrudan, J. Eriksson, and V. Koivunen, "Steepest descent algorithms for optimization under unitary matrix constraint," *IEEE Transactions on Signal Processing*, vol. 56, pp. 1134–1147, 3 2008. [Online]. Available: http://ieeexplore.ieee.org/document/4436033/

[44] T. Abrudan, J. Eriksson, and V. Koivunen, "Conjugate gradient algorithm for optimization under unitary matrix constraint," *Signal Processing*, vol. 89, pp. 1704–1714, 9 2009. [Online]. Available: https://linkinghub.elsevier.com/retrieve/pii/S0165168409000814

[45] D. Semmler, M. Joham, and W. Utschick, "High snr analysis of ris-aided mimo broadcast channels," in *2023 IEEE 24th International Workshop on Signal Processing Advances in Wireless Communications (SPAWC)*. IEEE, 9 2023, pp. 221–225. [Online]. Available: https://ieeexplore.ieee.org/document/10304487/

[46] G. H. Golub and C. F. V. Loan, *Matrix Computations*. Johns Hopkins University Press, 2013. [Online]. Available: https://jhupbooks.press.jhu.edu/title/matrix-computations

[47] R. Bhatia, "Linear algebra to quantum cohomology: The story of alfred horn's inequalities," *The American Mathematical Monthly*, vol. 108, pp. 289–318, 4 2001. [Online]. Available: https://www.tandfonline.com/doi/full/10.1080/00029890.2001.11919754

[48] L. Hogben, *Handbook of Linear Algebra*. CRC press, 2013.

[49] J. C. Gower and G. B. Dijksterhuis, *Procrustes Problems*. OUP Oxford, 2004. [Online]. Available: https://books.google.co.uk/books?id=kRRREAAAQBAJ

[50] T. Bell, "Global positioning system-based attitude determination and the orthogonal procrustes problem," *Journal of Guidance, Control, and Dynamics*, vol. 26, pp. 820–822, 9 2003. [Online]. Available: https://arc.aiaa.org/doi/10.2514/2.5117

[51] F. Nie, R. Zhang, and X. Li, "A generalized power iteration method for solving quadratic problem on the stiefel manifold," *Science China Information Sciences*, vol. 60, p. 112101, 11 2017. [Online]. Available: http://link.springer.com/10.1007/s11432-016-9021-9

[52] K. Gomadam, V. R. Cadambe, and S. A. Jafar, "A distributed numerical approach to interference alignment and applications to wireless interference networks," *IEEE Transactions on Information Theory*, vol. 57, pp. 3309–3322, 6 2011. [Online]. Available: http://ieeexplore.ieee.org/document/5773023/

[53] B. Clerckx and C. Oestges, *MIMO Wireless Networks: Channels, Techniques and Standards for Multi-Antenna, Multi-User and Multi-Cell Systems*. Elsevier Science, 2013. [Online]. Available: https://books.google.co.uk/books?id=drEX1J7jHUIC

[54] F. Negro, S. P. Shenoy, I. Ghauri, and D. T. Slock, "Weighted sum rate maximization in the mimo interference channel." IEEE, 9 2010, pp. 684–689. [Online]. Available: http://ieeexplore.ieee.org/document/5671658/